Journal of Chromatography, 626 (1992) 71–80
Elsevier Science Publishers B.V., Amsterdam

CHROM. 24 389

Flame-based thermionic detection coupled on-line with microcolumn liquid chromatography

II. Characterization of the system

Ch. E. Kientz and A. Verweij

Prins Maurits Laboratory TNO, P.O. Box 45, 2280 AA Rijswijk (Netherlands)

G. J. de Jong* and U. A. Th. Brinkman

Department of Analytical Chemistry, Free University, De Boelelaan 1083, 1081 HV Amsterdam (Netherlands)

ABSTRACT

Flame length and temperature measurements were used to study the influence of various parameter settings in thermionic detection coupled on-line with microcolumn liquid chromatography (micro-LC). In the present system both the rubidium source temperature and the interface performance depend strongly on the flame dimensions and gas flow-rates. When optimizing signal-to-noise ratios, the influences of the flame length, the rubidium source–burner rim distance and the hydrogen and air flow-rates are mutually dependent. When changing the micro-LC eluent composition from pure water to pure methanol, the noise and background are increasingly determined by chemi-ionization reactions.

INTRODUCTION

In a earlier study, thermionic detection (TID) with an instrument developed for gas chromatography (GC) was coupled to microcolumn liquid chromatography (micro-LC) [1]. For coupling, an interface was used that had earlier been designed for micro-LC with flame photometric detection [2,3]. This required minor modifications to both the interface and detector. The system was optimized by varying parameters such as the air, hydrogen and helium gas flow-rates, the rubidium (Rb) source–burner rim distance (see Fig. 5), the methanol content of the aqueous LC eluent and the eluent flow-rate. A minimum flame length of *ca.* 6 mm was found to be required to obtain stable eluent introduction and regular flame combustion; a near-stoichiometric H_2:O_2 ratio was found to give optimum detector sensitivity. The optimum Rb source–burner rim distance and the position of the eluent introduction capillary depended on the nature of the eluent. Mixtures of water and methanol were used; the highest sensitivity was obtained with pure methanol as eluent.

From the literature on GC–TID systems [4,5], it is well known that the operating mechanism of the detector is complicated and still awaits full elucidation. Spectroscopic [6] and mass spectral [7] studies are the best approaches to investigate the reaction products formed and to elucidate the reaction mechanisms involved. From studies on flame-based

Correspondence to: Professor U. A. Th. Brinkman, Department of Analytical Chemistry, Free University, De Boelelaan 1083, 1081 HV Amsterdam, Netherlands.

* Present address: Solvay Duphar BV, Analytical Development Department, P.O. Box 900, 1380 DA Weesp, Netherlands.

0021-9673/92/$05.00 © 1992 Elsevier Science Publishers B.V. All rights reserved

GC–TID it is known that the main factors affecting detector response are the temperature of both the flame and the alkali metal source [5]. When coupling micro-LC with a thermionic detector, the flame has an additional purpose: the temperature that is created by the flame is essential to transport the eluent and analytes into the flame [1], that is, temperature distribution and flame shape will largely determine the micro-LC-TID performance. The influence of the burner configuration, the detector gas flow-rates and the eluent introduction on the height and shape of and temperature distribution in the flame should therefore be well understood.

In this paper we attempt to explain the results of the optimization discussed in Part I [1] and briefly summarized above. To achieve this end, the influence of LC eluent introduction and detector gas flow-rate variation on the flame length and temperature distribution in different parts of the system (interface tip, flame, Rb source) was carefully investigated.

EXPERIMENTAL

Materials

All solvents were of HPLC grade from Merck (Darmstadt, Germany). PRP-1 polymer (10 μm) (Hamilton, Reno, NV, USA) was used as the column packing material. Dimethyl methylphosphonate was synthesized at the Prins Maurits Laboratory TNO. L-α-Lysophosphatidylethanolamine was supplied by Sigma (St. Louis, MO, USA).

Apparatus

The chromatographic system consisted of a Phoenix 20 CU pump (Carlo Erba, Milan, Italy), a Valco sample injection valve (VICI, Schenkon, Switzerland) with a 60-nl internal volume and a thermionic detector (Carlo Erba). The various fused-silica connection tubings (0.02–0.3 mm I.D.) were supplied by Chrompack (Middelburg, Netherlands).

The 150 mm × 0.3 mm I.D. fused-silica microcolumn was packed with PRP-1 according to the procedure of Gluckman *et al.* [8]. The column performance was tested using a Spectroflow 783 UV detector (Kratos ABI Analytical, Ramsey, NJ, USA) assembled with a laboratory-made 40-nl micro-UV flow cell [9].

The detector and interface were described in detail in Part I [1].

Flame measurement

The colourless hydrogen–air flame was made visible with the use of a small piece of sodium glass. Its height was measured against a dark background.

Flame temperatures were measured with the use of a laboratory-made platinum *versus* platinum–10% rhodium thermocouple (2 mm × 0.1 mm O.D.) insulated with a 100 mm × 1.4 mm O.D. ceramic rod. The temperature range of this thermocouple extends to 1700°C (*cf.* standard calibration tables for thermocouples [10]).

RESULTS AND DISCUSSION

Flame characteristics

From the literature on flame combustion [11], it is well known that the simplest form of diffusion flame will occur when a fuel jet flows from a small-diameter burner tube into air of about the same velocity in a wider concentric tube. The majority of the burners used in flame-based GC detectors such as the thermionic and flame photometric detector are constructed according to this principle. The flame originates at the rim of the burner tube, which in this study was the inner glass tube of the modified interface–burner head. It is also known that the shape of the flame surface is determined by the rapidity of the mixing of hydrogen and air and depends on whether air is in excess (overventilated flame; the surface is closed) or is deficient (underventilated flame; the surface has the shape of a cup, called an open or inverted flame shape).

Depending on the gas flow-rates used, mixing takes place by means of laminar or turbulent diffusion. With the hydrogen flow-rates generally applied in GC detector burners, the diffusion flames are laminar (Reynolds number <2000). With laminar flames mixing is controlled by molecular diffusion. The length (L, cm) to achieve a specified, degree of mixing is directly proportional with the volumetric flow (V, cm^3/s) and inversely proportional to the diffusion coefficient of hydrogen in air (D, 0.63 cm^2/s). The flame length can be derived from the relationship [11]

$$L = V/\pi D \quad (1)$$

which indicates that the flame length is independent of the burner diameter if the flame is laminar. We checked the validity of eqn. 1 for small flames (length 2–25 mm) in an experiment in which the flame length (visible by the yellow emission of the sodium glass) was measured at different hydrogen flow-rates for burner diameters of 0.5–1 mm I.D. Fig. 1 shows that the values calculated from eqn. 1 are close to those observed experimentally. It also shows that the presence of the fused-silica capillary placed inside the 0.7 mm I.D. burner tip of the interface (without solvent introduction into the flame) does not change the flame length.

The influence of the helium flow-rate (60–150 ml/min) and air flow-rate (from ambient to *ca.* 600 ml/min) on the flame shape was negligible; the flame shape remained essentially the same with a length of 9.0 ± 0.5 mm and a maximum diameter of 4 ± 0.5 mm (hydrogen flow-rate 95 ml/min).

In this study, increasing the methanol flow-rate (range 0–15 μl/min) caused a linear increase in temperature as measured at different positions of 5–12 mm above the burner rim, *i.e.*, partly in and partly above the flame (Fig. 2). The flame length also increased linearly when increasing the flow-rate of methanol. However, it remained constant when introducing increasing amounts of water, aqueous 0.5 *M* ammonium acetate or 0.5 *M* ammonium formate in the range of 5–15 μl/min. The increase in the flame temperature due to methanol introduction was found to be independent of the hydrogen flow-rate used (Fig. 3). On introducing water, the temperature profile was the same as for the reference measurements without solvent introduction, again irrespective of the hydrogen flow-rate used (Fig. 3).

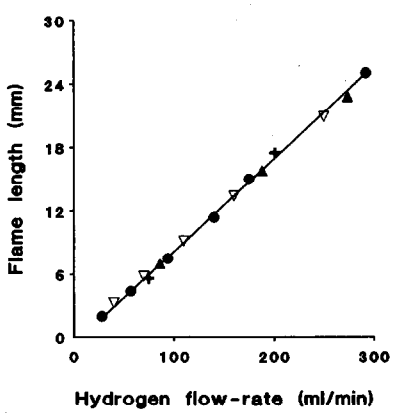

Fig. 1. Influence of hydrogen flow-rate on flame length for different internal diameters of the burner of (▲) 0.5, (●) 0.7 (interface–burner head) and (+) 1 mm. ▽ = data calculated according to eqn. 1. Air, ambient.

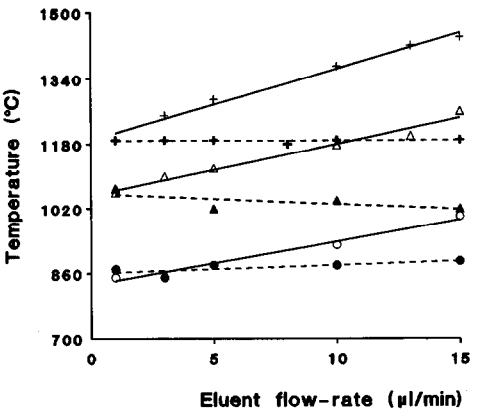

Fig. 2. Influence of the LC eluent flow-rate on temperature measured at various heights above the burner rim: + = 5; ▲ = 7; △ = 8; ● = 10; ○ = 12 mm. Eluent: ———, methanol; – – –, water. Flame length, 9 mm; hydrogen flow-rate, 95 ml/min; helium flow-rate, 100 ml/min; air, ambient.

Fig. 4 shows the relationship between the temperature in and above the flame (flame length 9 mm) measured at various heights above the burner rim when introducing either methanol or water at a constant flow-rate of 10 μl/min. The results are compared with the temperature distribution without

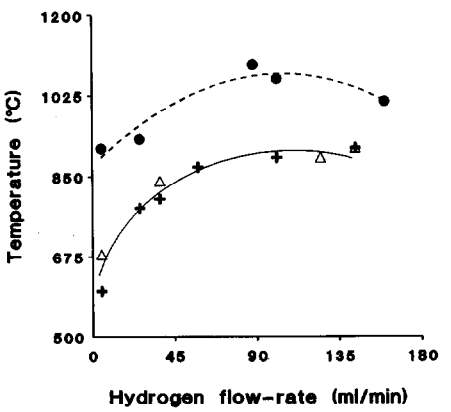

Fig. 3. Influence of LC eluent (methanol) on the flame temperature measured at various hydrogen flow-rates. Temperature measured at 10 mm length above the burner rim; helium flow-rate, 100 ml/min; air, ambient; LC eluent flow-rate, 10 μl/min. Reference temperature measurements were made without eluent introduction. + = Reference; ● = methanol; △ = water.

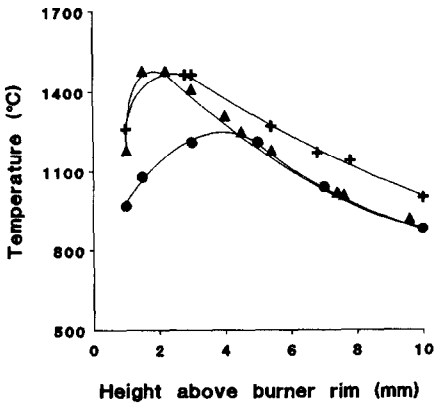

Fig. 4. Influence of LC eluent (methanol or water) on flame temperature at various lengths above the burner rim. The reference temperature measurement was made without eluent introduction. LC eluent flow-rate, 10 μl/min; flame length, 9 mm; hydrogen flow-rate, 95 ml/min; helium flow-rate, 100 ml/min; air, ambient. ▲ = Reference; + = methanol; ● = water.

solvent introduction. Obviously, for heights above the burner rim of over 3 mm the excess of heat released by the combustion of methanol causes a temperature increase. With water as solvent the temperature measured at heights above the burner rim of over 5 mm is the same as without solvent introduction. At lower heights low temperatures are found compared with the flame temperature without solvent introduction. This may be due to conversion of liquid water into gas, and suggests that the solvent leaves the interface capillary as a liquid.

Interface operation

It is interesting to compare the phenomena observed on solvent introduction into the interface used in this study (Fig. 5) with those reported for direct liquid introduction interfaces and thermospray units in mass spectrometry [12–15]. According to Vestal and co-workers [13,14], a thermospray unit can be described as a supersonic jet of vapour with entrained particles or droplets, generated by applying enough heat to a capillary to effect partial vaporization of a liquid as it passes through the capillary. With linear flow velocities of about 80–150 cm/s and a *ca.* 0.1 mm I.D. capillary, the typical thermospray operating point occurs between 150 and 250°C. In our study the temperature measured at the tip of the helium-cooling capillary outlet (see

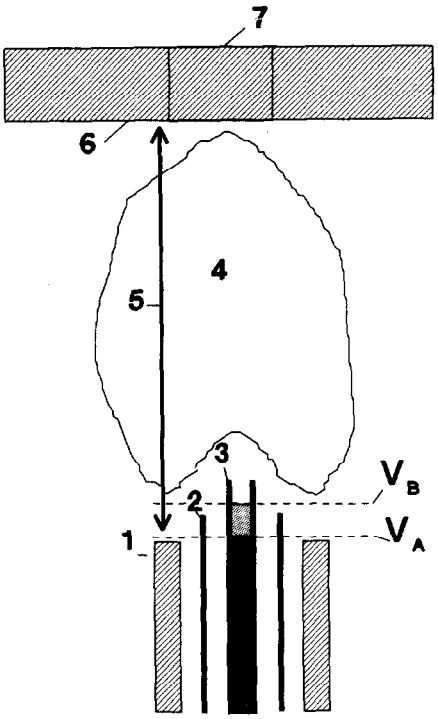

Fig. 5. Schematic diagram of interface configuration (not drawn to scale). 1 = Burner rim; 2 = 0.32 mm I.D. fused-silica helium introduction capillary; 3 = 0.1 mm I.D. eluent introduction capillary; 4 = flame; 5 = Rb source–burner rim distance; 6 = Rb source; 7 = Rb source cavity; V_A–V_B = vaporization zone. For further details, see text.

No. 2 in Fig. 5) proved to be 700°C at a helium flow-rate of about 100 ml/min [1], which is much higher than the temperature quoted above. Moreover, with the interface used in this study, which also contains a *ca.* 0.1 mm I.D. eluent introduction capillary (No. 3 in Fig. 5), the linear solvent flow velocity is only *ca.* 2 cm/s. In conclusion, the interface does not operate as a thermospray and complete vaporization is expected to occur.

For direct liquid interfaces, according to Arpino and Beaugrand [15] the volume flow-rate of vaporization, F (ml/min), in the capillary is

$$F = \frac{\pi P_v}{\rho} \cdot \frac{d_0^2}{2} \left(\frac{M}{2\pi RT} \right)^{1/2} \quad (2)$$

where P_v is the saturated vapour pressure of the LC eluent at temperature T, d_0 is the diameter of the liquid introduction capillary, M and ρ are the molecular weight and the density of the liquid,

respectively, and R is the gas constant. Assuming the temperature at V_A (see Fig. 5) to be 100°C, one can calculate from eqn. 2 that the vaporization rate of water is at least ten times higher than the input of 10 μl/min. As a consequence, vaporization might occur prematurely, *i.e.*, deep inside the capillary, causing non-volatile analytes to be deposited in the capillary. However, the position of the solvent meniscus in the eluent introduction capillary, which was observed to be continuously fluctuating between V_A and V_B, *i.e.*, within the vaporization zone, shows that the helium cooling prevents vaporization to occur deeper than about 0.5–1 mm inside this capillary. The observed fluctuation of the vaporization zone suggests a plug-type solvent introduction into the flame[a].

The above suggestion is supported by the relatively low flame temperature measured close to the exit of the eluent introduction capillary in the case of water (see Fig. 4). Such interface operation should allow the introduction of even distinctly non-volatile analytes into the flame. As an illustration of the potential of the present system to handle such analytes, an LC–TID trace for the phospholipid L-α-lysophosphatidylethanolamine is shown in Fig. 6.

At constant eluent flow-rate, the position of the vaporization zone V_A–V_B (Fig. 5) depends on the vapour pressure of the solvent and the temperature. With an eluent having a low vapour pressure and low specific heat capacity such as water, V_A–V_B will be situated high up in the capillary or even above the outlet of the eluent introduction capillary. Consequently, the LC eluent will leave the capillary as a liquid flowing over its tip, as was indeed observed by us, and will not be introduced into the flame. In order to prevent this, the capillary has to be moved into a higher temperature position. In Fig. 4 it was shown that the maximum temperature occurs *ca.* 2 mm above the burner rim. In other words, the capillary has to be moved closer to the flame. This explains the necessity to increase the eluent introduction capillary–burner rim distance (by *ca.* 0.5 mm) when using water instead of methanol, as was discussed previously [1]. Actually, proper interface operation can also be restored while maintaining the initial eluent introduction capillary–burner rim distance, *viz.*, by changing the temperature of the gas mixture surrounding the capillary. On decreasing the helium gas flow-rate, F, from *ca.* 100 to *ca.* 50 ml/min, the temperature, T at the capillary tip will increase from *ca.* 700 to *ca.* 900°C, as can be calculated from the relationship $T = -4F + 1115$ [1]. In other words, changing the helium flow can be used to optimize eluent introduction when the eluent composition and hence the boiling point of the mixture have been changed.

Thermionic detector operation

In order to study the influence of the detector gas flow-rates on the TID characteristics, a volatile test compound, dimethyl methylphosphonate (DMMP), was selected because it shows a TID response that is independent of the mode of introduction (liquid or vapour) into the flame.

Hydrogen flow-rate. As shown in eqn. 1, at a constant air flow-rate the flame length and, con-

[a] The fluctuation of the vaporization zone can be tentatively explained as follows. When the meniscus has retracted inside the capillary to V_A, the pressure is atmospheric (P_0), because the pressure inside the detector may be assumed to be equal to the outside pressure. The solvent delivered at V_A evaporates completely and the vapour pressure above the solvent starts to increase (P_v). Owing to expansion (a flow of 10 μl/min of water produces 12 ml/min of vapour) and the steep temperature increase (from 100°C, which is the eluent boiling point at P_0, to 700°C), the pressure increase (P_0 to P_V) is dramatic [10]. The increasing pressure reduces the vaporization rate, the solvent becomes overheated and the vaporization zone moves to V_B. At V_B the pressure is assumed to have been reduced sufficiently (because the gas column is pushed out of the capillary by the solvent moving from V_A to V_B) to release the overheated solvent volume between V_A and V_B, restoring the vaporization zone to V_A and reducing the pressure to P_0.

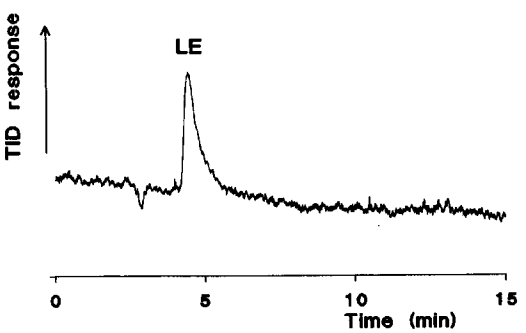

Fig. 6. Micro-LC–TID of 10 ng of L-α-lysophosphatidylethanolamine (LE). Column, 150 mm × 0.32 mm I.D. packed with PRP-1; eluent, methanol–water–formic acid (95:5:0.5); flow-rate, 8 μl/min.

sequently, the position of the high-temperature zone in the flame depend on the hydrogen flow-rate. That is, varying the hydrogen flow-rate results in (i) a different flame–Rb source distance (a 50–100 ml/min increase of the hydrogen results in an about 4 mm increase of the flame length as calculated from eqn. 2), (ii) a different H_2:O_2 ratio and (iii) an inverted flame shape, if hydrogen is in excess. These changes should be carefully considered when interpreting the results obtained on varying the hydrogen flow-rate.

The influence of the hydrogen flow-rate on the analyte signal, and the noise, signal-to-noise (S/N) ratio and temperature measured in the cavity of the Rb source is shown in Fig. 7. Increasing the hydrogen flow-rate from 80 to 100 ml/min (this range corresponds with an H_2:O_2 ratio slightly over the stoichiometric value of 2.0) gave a distinct decrease of both signal and noise. However, the Rb source surface temperature (data not shown) and the temperature in the Rb source cavity (see Fig. 7) just above the flame remained essentially constant. This may indicate that the analyte signal, and also the noise level (see next section), is primarily determined by chemi-ionization reactions in the flame, and not by the temperature. Recently, using mass spectrometry, Bombick and Allison [4] found that PO_3^- is the most abundant ion produced by the interaction of organophosphorus compounds with a hot alkali-ceramic bead. The PO_3^- ion may well be the charge carrier that causes the TID response [4]. For the reductive mode of the flame as used with the flame photometric detector, it is well known that the neutral molecule HPO is responsible for the green phosphorus emission. Possibly, when there is an excess of hydrogen, part of the PO_3^- ions is converted into neutral HPO molecules, which will result in a lower signal.

At low hydrogen flow-rates the flame is overventilated and will be relatively hot (see next section and Fig. 8). However, it will also be short (see eqn. 1). Therefore, the temperature of the reaction gas mixture in the cavity of the Rb source decreases and there is a simultaneous strong decrease in signal (Fig. 7); this suggests a dependence of analyte signal on temperature. In other words, a decreasing hydrogen flow-rate causes a lower flame position; this in its turn results in a decreased Rb source temperature and a correspondingly lower signal. The noise, however, remains essentially constant and the S/N ratio will consequently decrease sharply. These results concerning overventilated flames confirm the mutual dependence of the optimum Rb source–rim distance and the hydrogen flow-rate discussed previously [1].

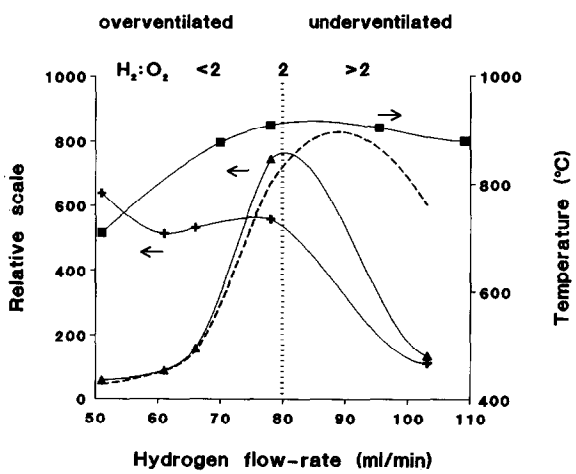

Fig. 7. Influence of hydrogen flow-rate on signal, S/N ratio, noise and Rb source cavity temperature. Air flow-rate, 200 ml/min; eluent, methanol; flow-rate, 10 μl/min. ▲ = Signal; + = noise; ■ = Rb source cavity temperature. Dashed line, S/N ratio.

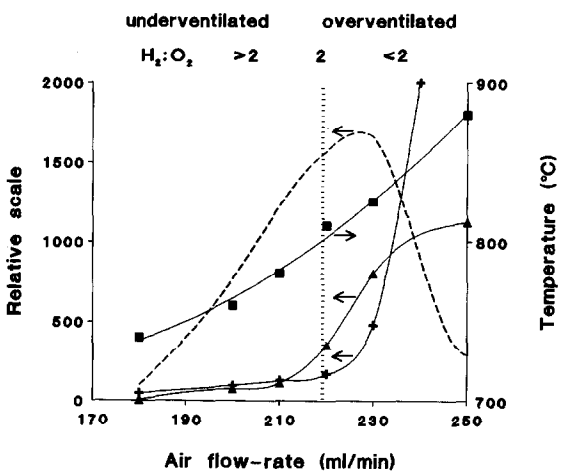

Fig. 8. Influence of air flow-rate on signal, noise, S/N ratio and Rb source cavity temperature. Hydrogen flow-rate, 88 ml/min; analyte, DMMP; eluent, methanol; flow-rate, 10 μl/min. ▲ = Signal; + = noise; ■ = Rb source cavity temperature. Dashed line, S/N ratio.

Air flow-rate. When varying the air flow-rate (at a constant hydrogen flow-rate of 95 ml/min), the flame length will remain constant, as discussed in the section on the flame characteristics. That is, whereas a hydrogen flow-rate variation changes both flame length and H_2:O_2 ratio, in the case of an air flow-rate variation only the H_2:O_2 ratio will vary; consequently, a change in the Rb source cavity temperature is expected. In Fig. 8 (eluent methanol) the influence of the air flow-rate on analyte signal, noise, S/N ratio and Rb source cavity temperature is shown. The optimum S/N ratio at an air flow-rate of 220–230 ml/min (hydrogen flow-rate 88 ml/min) corresponds to a H_2:O_2 ratio of *ca.* 1.95. As shown in Fig. 8, the temperature increases with increasing air flow-rate up to at least 250 ml/min. The detector noise is relatively low and constant above the stoichiometric H_2:O_2 ratio, *i.e.*, when oxygen is deficient. Just below the stoichiometric ratio (air flow-rate >220 ml/min), the analyte signal, noise level (and background; data not shown) start to increase sharply. On further increasing the air flow-rate (H_2:O_2 ratio decreasing from 2 to 1.5), the analyte signal decreases but the noise and background remain relatively high, as shown in Fig. 7, here and Fig. 3A–C in ref. 1. This means that, with methanol as eluent, the noise level essentially determines the optimum S/N ratio.

With water instead of methanol (data not shown), the background and noise remained constant over the total air flow-rate range of 150–300 ml/min (H_2:O_2 ratio from 3 to 1.5). Here the noise is probably the result of the eluent introduction. This suggests that the strong increase of noise and background is the result of the presence of organic molecules (methanol) in the LC eluent, *i.e.*, of the formation of organic ions due to chemi-ionization:

$$CH + O \rightarrow CHO^+ + e^- \quad (3)$$

followed by a charge-exchange reaction:

$$CHO^+ + H_2O \rightarrow H_3O^+ + CO \quad (4)$$

The hydronium ion, H_3O^+, is known to be the dominant ion in hydrocarbon flames [9]. It may decay by reactions such as:

$$H_3O^+ + e^- \rightarrow H_2O + H \quad (5)$$

Eqns. 3 and 4 may explain the relationship between the formation of organic ions and the flame mode when using methanol as eluent.

In the case of overventilation, eqn. 3 shows the initiation of the reaction via the presence of oxygen radicals. The hydrogen radicals formed according to eqn. 5 will be consumed by oxygen [5]:

$$H + O_2 \rightarrow OH + O \quad (6)$$

In other words, overventilation causes the formation of ions and thus increases the noise and background. On the other hand, when the flame is underventilated and hydrogen is in excess, the oxygen radicals will be consumed and hydrogen radicals will be formed, as shown in the equations [5]

$$O + H_2 \rightarrow OH + H \quad (7)$$

$$OH + H_2 \rightarrow H_2O + H \quad (8)$$

This may explain the sharp decrease in noise and background observed when the H_2:O_2 ratio is above the stoichiometric value of 2.0; the consumption of oxygen radicals by hydrogen according to eqns. 7 and 8 prevents the initiation reaction (eqn. 3) from occurring and, consequently, the formation of CHO^+ and H_3O^+ ions.

Hydrogen/air flow-rate ratio. The above results indicate that when keeping the H_2:O_2 ratio constant at the stoichiometric ratio, varying the hydrogen flow-rate will simply result in a change in flame length (see eqn. 1). That is, the simultaneous variation of the hydrogen and air flow-rates over not too large a range has a similar effect as varying the Rb source–burner rim distance. Alternatively, when the flame length and the Rb source–burner rim distance are simultaneously increased to the same extent, the position of the flame boundary relative to the Rb source, and hence the Rb source temperature, is expected to remain essentially constant. This will result in a relatively constant S/N ratio, as was indeed observed previously [1] for a simultaneous hydrogen and Rb source–burner rim distance increase of *ca.* 10 ml/min and *ca.* 0.5 mm, respectively (using adjusted air flow-rates to maintain a constant H_2:O_2 ratio of 1.95).

In contrast to the above, an increase in the S/N ratio occurred when the hydrogen (and air) flow-rates and the Rb source–burner rim distance were simultaneously increased over a much wider range. Fig. 9 shows the increase in the S/N ratio (see arrow) on simultaneously increasing the Rb source–burner rim distance by 6 mm and the hydrogen flow-rate by 70 ml/min (a 70 ml/min increase corresponds to a 6

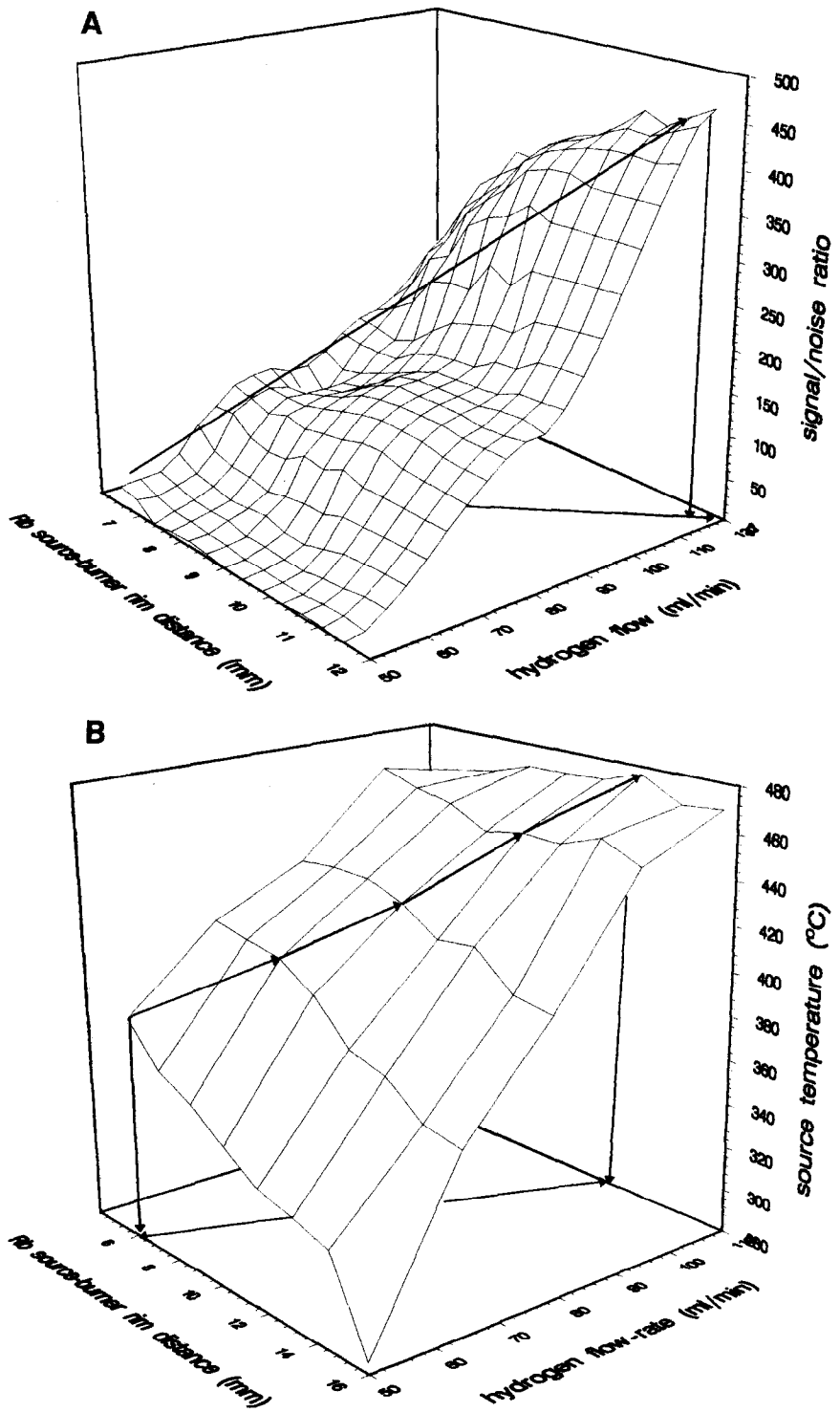

Fig. 9. (A) Dependence of signal-to-noise ratio on hydrogen flow-rate and Rb source–burner rim distance. H_2:O_2 ratio, 1.95. (B) Dependence of Rb source temperature on hydrogen flow-rate and Rb source–burner rim distance. H_2:O_2 ratio, 1.95.

mm increase in flame length; *cf.* eqn. 1). The data presented in Fig. 5A (analyte signal) and Fig. 5B (noise) in ref. 1 may be used to explain why the S/N ratio decreases dramatically both in front of and behind the triangular plane shown in Fig. 9A here. There is a marked parallellism between the optimum S/N ratio plot in Fig. 9A and the plot illustrating the Rb source temperature increase (Fig. 9B). The increase in the source temperature is probably the result of the increased thermal energy of the flame, which is directly proportional with the hydrogen flow-rate.

It should be added that the present detector configuration requires modification to allow convenient handling of some of the large flames and Rb source–burner rim distances used above.

CONCLUSIONS

The characterization of the micro-LC–TID system attempted in this paper clearly shows that the temperature of the Rb source depends strongly on the flame dimensions and gas flow-rates used. A high temperature of the surface and cavity of the Rb source appears essential to obtain a strong analyte signal. The flame should come close to the Rb source without, however, enveloping it, because this will cause a dramatic increase in the noise level. In other words, the optimum distance essentially equals the flame length.

As the flame length depends on the hydrogen flow-rate, provided the H_2:O_2 ratio is <2, the Rb source–burner rim distance and hydrogen flow-rate are mutually dependent. Further, the analyte signal depends strongly on the hydrogen and air flow-rates, and reaches its maximum at a H_2:O_2 ratio close to the stoichiometric value, *i.e.*, in the range 1.90–2.05. These results hold true for all methanol–water mixtures irrespective of their composition. However, on increasing the methanol content of an aqueous–organic eluent, the flame length will increase. The concomitant increase in noise and background is probably the result of chemi-ionization reactions rather than temperature effects. Self-evidently, if the methanol content of an eluent is increased, the Rb source–burner rim distance will have to be increased in order to maintain optimum conditions.

The configuration of the present interface with its continuously fluctuating vaporization zone allows the introduction of both volatile and non-volatile analytes into the flame, that is, it meets the main demand required of an interface between an LC separation and a GC-type detection system.

Finally, considering the situation from a practical point of view, one should realize that the mutual dependence of almost all parameters involved, hydrogen and air flow-rates, Rb source–burner rim distance and nature of the solvent, results in a system that is sensitive to small changes in operating conditions. Careful optimization of the system is therefore required, especially when the chromatographic conditions are changed. Uncoupling the regulation of the Rb source temperature and the flame temperature by introducing an external heating unit will certainly result in a less complicated system. In view of the promising analytical results already obtained with the present system, this will be an interesting subject for future studies on micro-LC–TID. Its implementation should facilitate the use of thermionic detection in LC.

ACKNOWLEDGEMENTS

The authors are greatful to A. C. van de Berg and C. J. de Ruiter for helpful discussions.

REFERENCES

1 Ch. E. Kientz, A. Verweij, G. J. de Jong and U. A. Th. Brinkman, *J. Chromatogr.*, 626 (1992) 59.
2 Ch. E. Kientz, A. Verweij, H. L. Boter, A. Poppema, R. W. Frei, G. J. de Jong and U. A. Th. Brinkman, *J. Chromatogr.*, 467 (1989) 385.
3 Ch. E. Kientz, A. Verweij, G. J. de Jong and U. A. Th. Brinkman, *J. High Resolut. Chromatogr.*, 12 (1989) 793.
4 G. Guiochon and C. L. Guillemin (Editors), *Quantitative Gas Chromatography*, Elsevier, Amsterdam, 1988.
5 M. Dressler (Editor), *Selective Gas Chromatographic Detectors*, Elsevier, Amsterdam, 1986.
6 P. van de Weijer, B. H. Zwerver and R. J. Lynch, *Anal. Chem.*, 60 (1988) 1380.
7 D. D. Bombick and J. Allison, *J. Chromatogr. Sci.*, 27 (1989) 612.
8 J. C. Gluckman, A. Hirose, V. L. McGuffin and M. Novotny, *Chromatographia*, 17 (1984) 3039.
9 Ch. E. Kientz and A. Verweij, *J. High Resolut. Chromatogr. Chromatogr. Commun.*, 3 (1988) 294.
10 D. R. Lide (Editor), *CRC Handbook of Chemistry and Physics*, CRC Press, Boston, MA, 72nd Ed., 1991–92, p. 15-1.
11 B. Lewis, *Combustion, Flames and Explosions of Gases*, Academic Press, Orlando, FL, 1987, p. 479.

12 A. P. Bruins and B. F. H. Drenth, *J. Chromatogr.*, 271 (1983) 271.
13 C. R. Blakley and M. L. Vestal, *Anal. Chem.*, 55 (1983) 750.
14 M. L. Vestal and G. J. Fergusson, *Anal. Chem.*, 57 (1985) 2378.
15 P. J. Arpino and C. Beaugrand, *Int. J. Mass Spectrom. Ion Processes*, 64 (1985) 275.